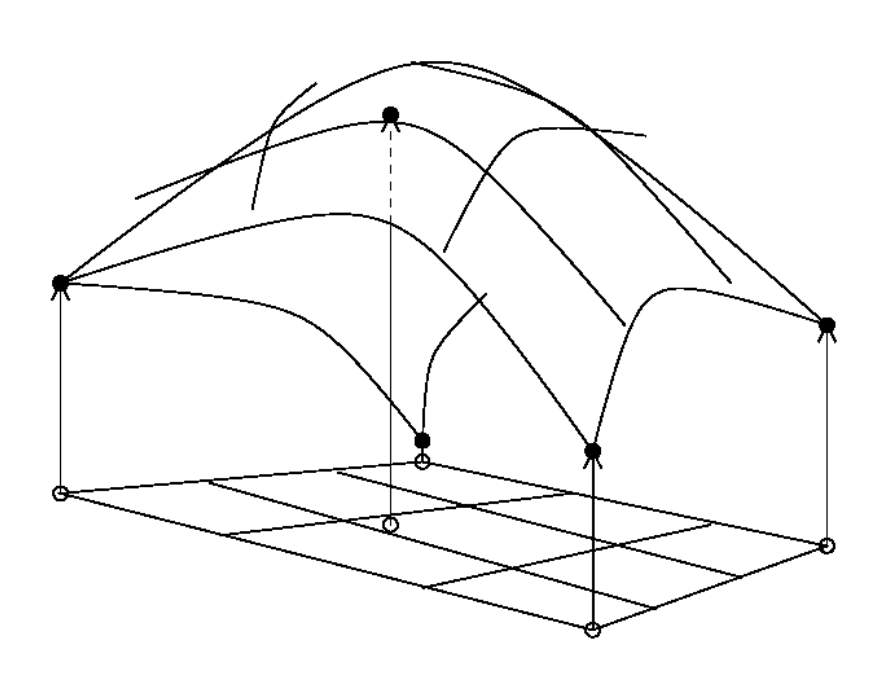
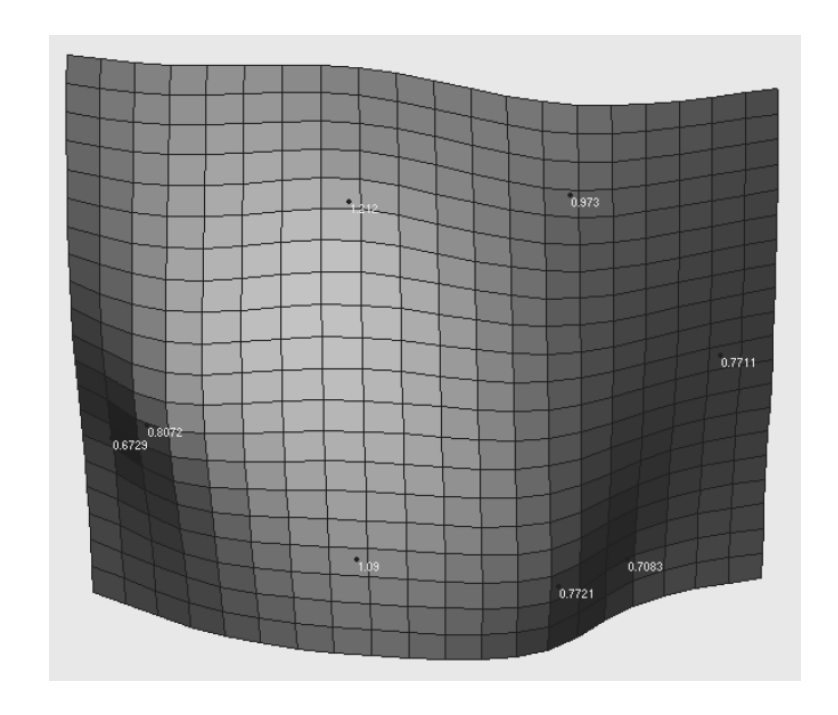
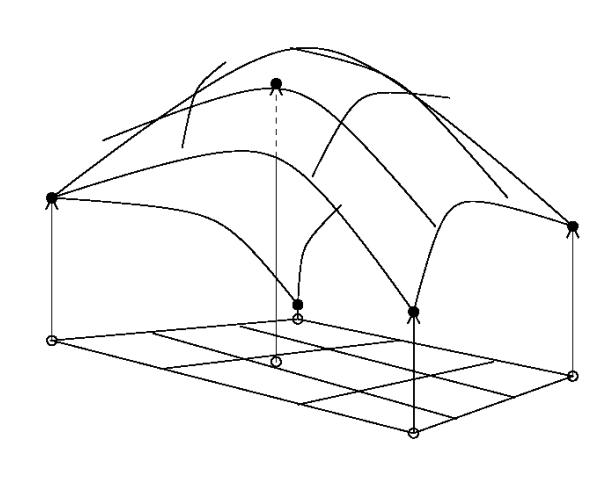
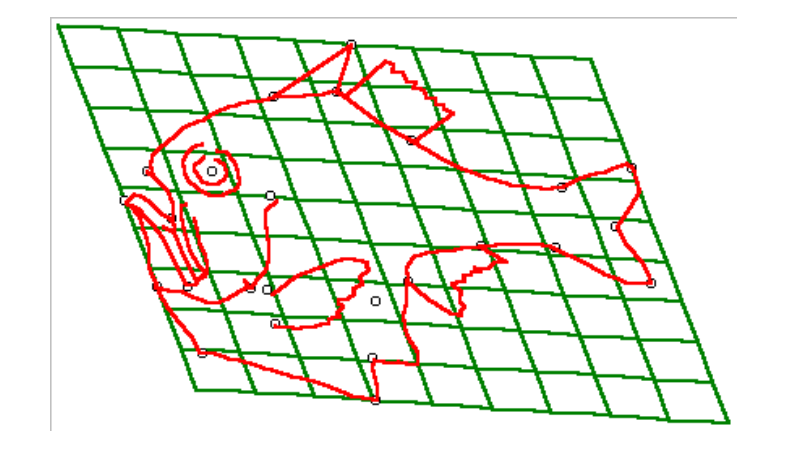
This method is based on the model of deformation of an infinite and infinitely thin metal plate. A coordinate grid (an imaginary metal plate) is placed on the reference object and then shaped to match the compared object. The differences between the objects are represented by the deformation of the originally rectangular grid or the flat metal plate

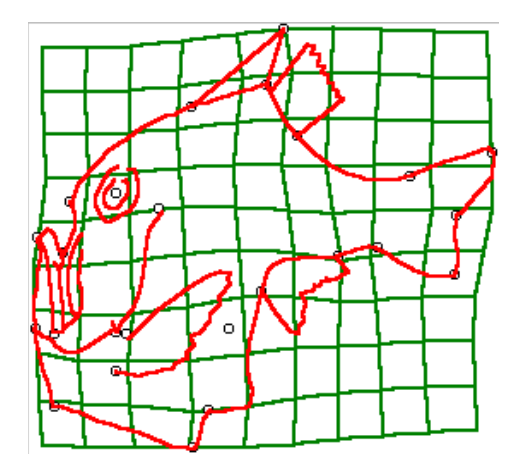




The change in the position of landmarks on a surface defined by the x and y axes relative to the reference object is displayed either by tilting or rotating the surface (metal plate) or by its bending. When bent, the change appears along the third axis – the z-axis (the plate can no longer remain flat).



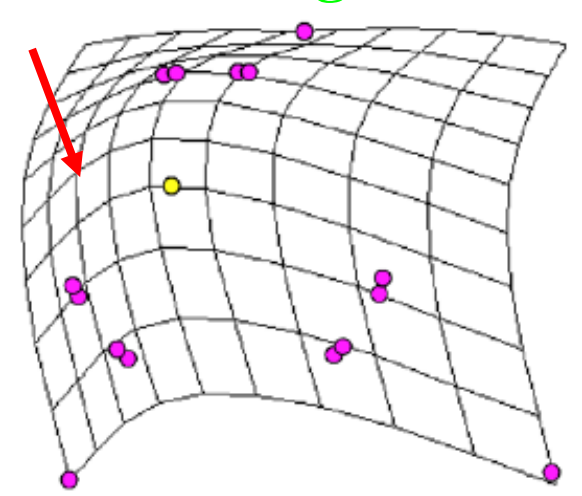


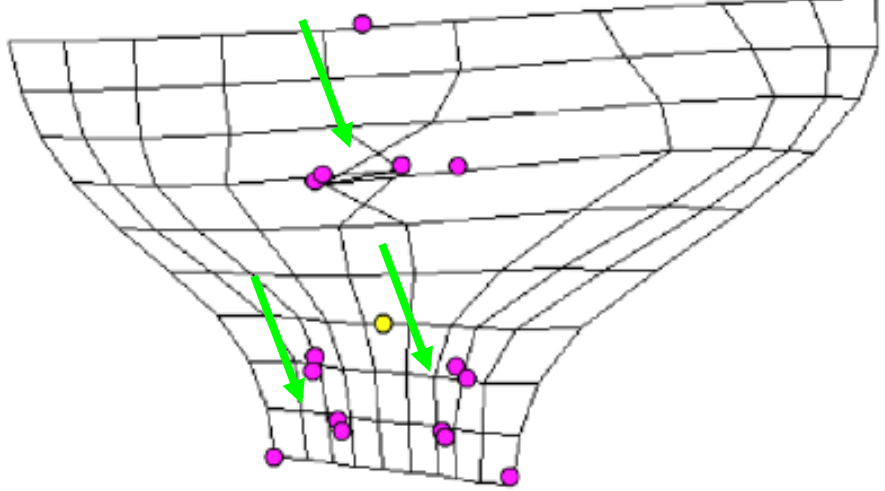


The degree of bending of the metal plate is expressed by the amount of energy required to bend the plate (deformation energy, bending energy). The more localized the deformation of the plate, the higher the required deformation energy. Unlike Procrustes analysis, deformation energy cannot be interpreted as a measure of the difference between compared objects, but rather as a measure of the locality of shape changes.

less localized changes – less energy

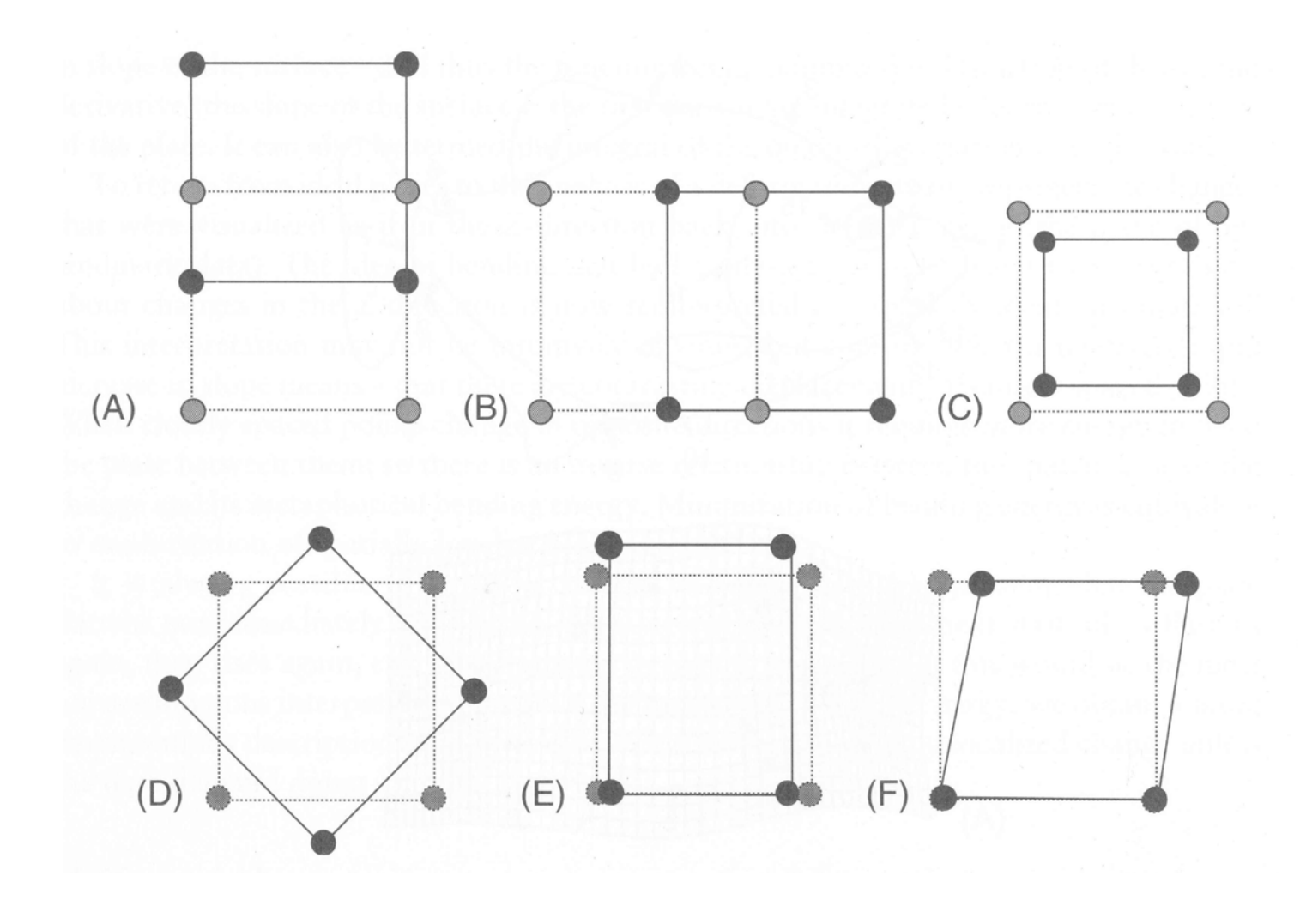
localized changes – more energy





MacLeod (2001)

The change in the shape of an object, or the differences between the shapes of two objects, can be decomposed into an affine component (affine, linear transformation), where changes occur along one of the orthogonal axes while maintaining the parallelism of lines in the original coordinate grid, and a nonaffine component (non-affine, non-linear transformation), where deformation of the coordinate grid lines occurs. The affine component of changes includes all transformations of size, rotation, and also homogeneous compression or elongation of the shape in one direction. The deformation energy for the affine component of changes is zero because there is no bending of the imaginary metal plate. The non-affine component of changes affects each landmark differently.



A – translation along the vertical axis, B – translation along the horizontal axis, C – scaling, D – rotation, E – compression/dilation, F – tilting

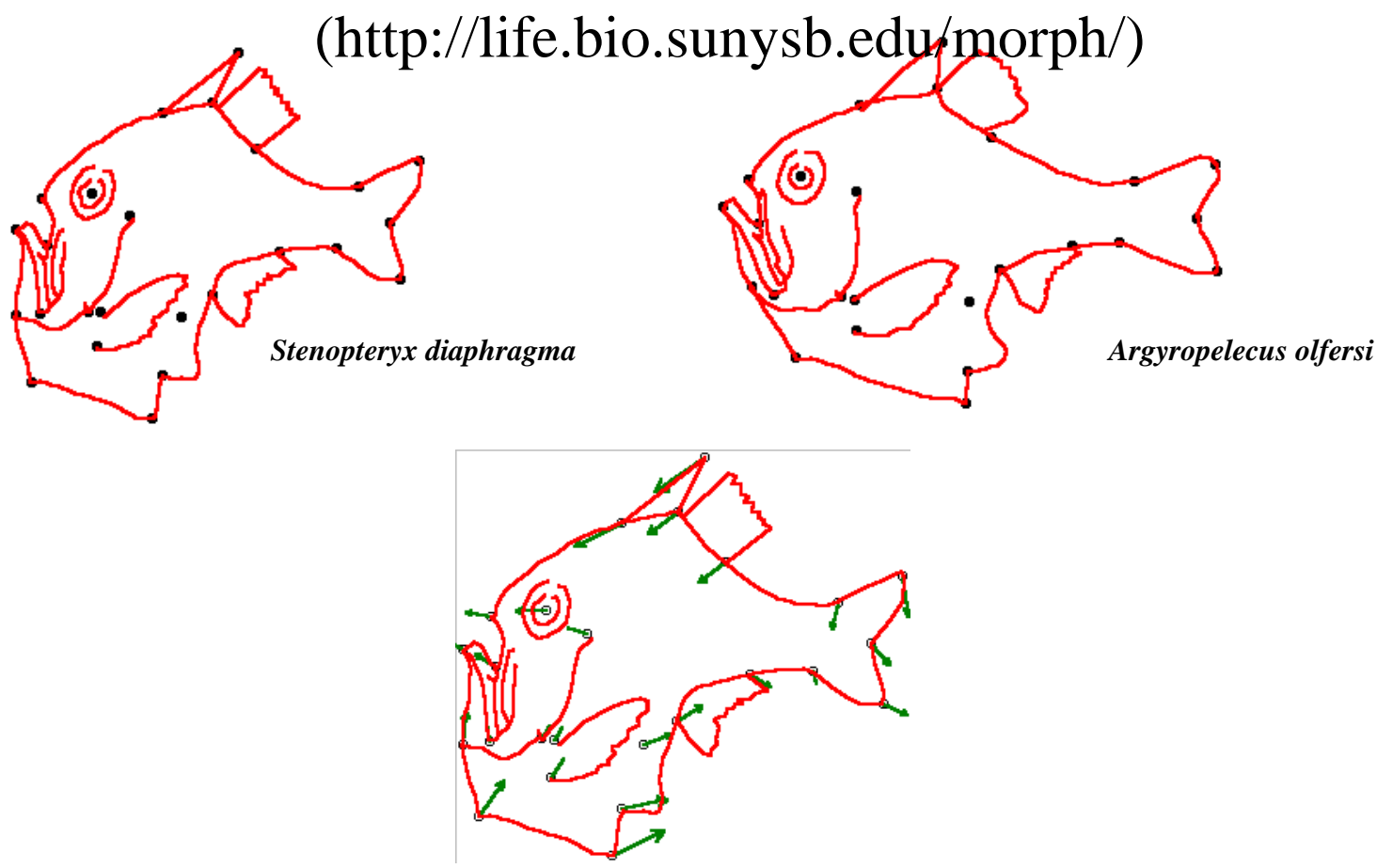
#### Zelditch et al. (2004)

Mutual shape relationships of the species

Stenopteryx diaphragma and Argyropelecus olfersi

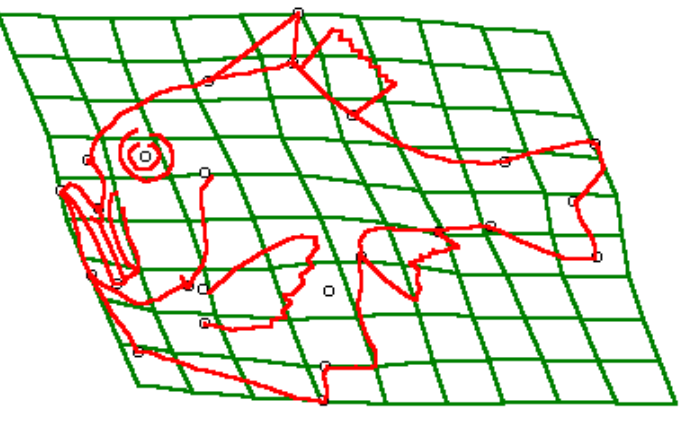
Sample data from the tpsSpline program

(http://life.bio.sunysb.edu/morph/)

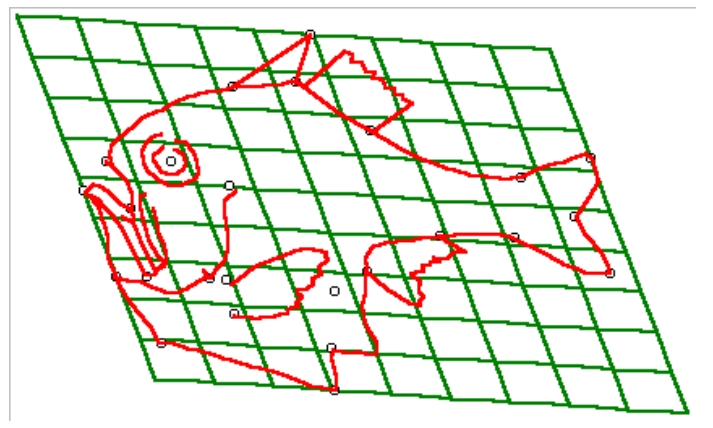


Relationships expressed using vectors

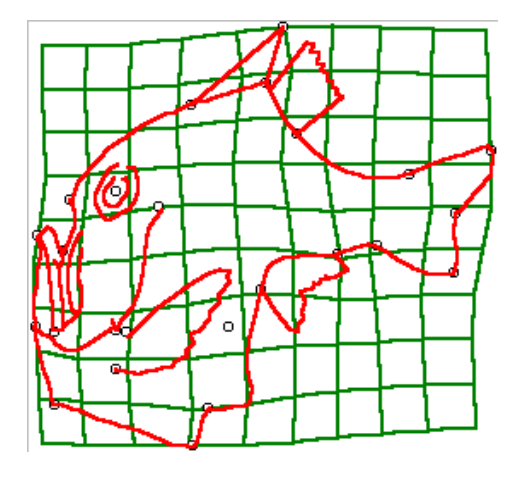
## Mutual shape relationships of the species Stenopteryx diaphragma and Argyropelecus olfersi



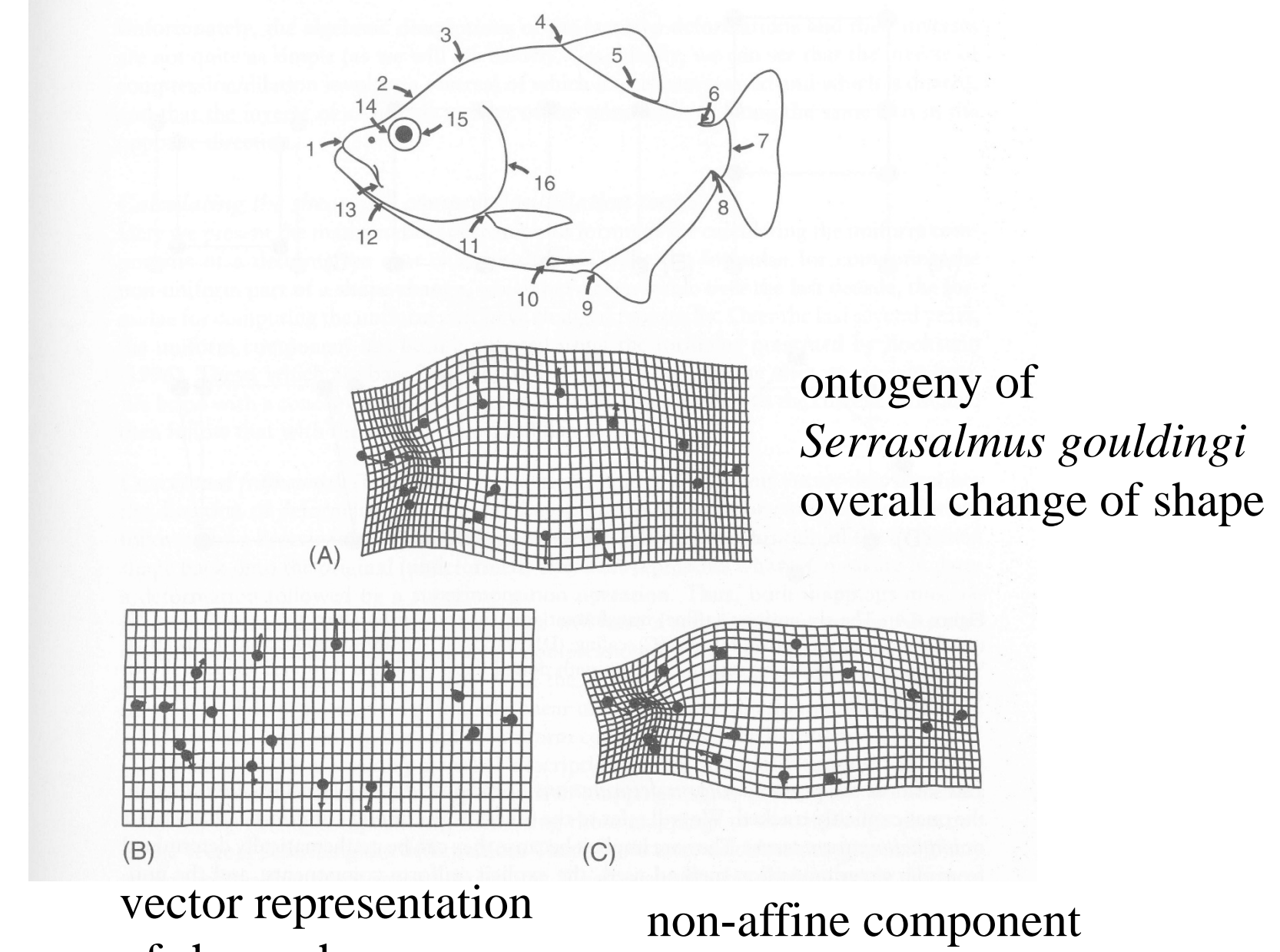
overall change of shape



affine component of shape change



non-affine component of shape change



of shape change

of shape change

Zelditch et al. (2004)

- •At the beginning of the analysis using the thin-plate spline method, we select a reference object. This may be a younger ontogenetic stage, a presumed evolutionary ancestor, or an average configuration determined by the Procrustes method.
- •From the reference object, we calculate the deformation energy matrix (bending energy matrix),  $\mathbf{L}_{p}^{-1}$  where p is the number of landmark points.
- •This matrix is a function of the distances between the landmark points in the reference object.

For the matrix 
$$\mathbf{L}$$
, it holds that  $\mathbf{L} = \begin{bmatrix} \mathbf{P} & \mathbf{Q} \\ \mathbf{Q}^{t} & \mathbf{0} \end{bmatrix}$ 

where 0 is a 3 x 3 matrix of zeros, further

$$\mathbf{P} = \begin{bmatrix} 0 & U(r_{12}) & U(r_{13}) & \dots & U(r_{1p}) \\ U(r_{21}) & 0 & U(r_{23}) & \dots & U(r_{2p}) \\ U(r_{31}) & U(r_{32}) & 0 & \dots & U(r_{rp}) \\ \vdots & \vdots & \vdots & \ddots & \vdots \\ U(r_{p1}) & U(r_{p2}) & U(r_{p3}) & \dots & 0 \end{bmatrix}$$

where the function U is defined  $U(r_{ij}) = r_{ij}^2 \ln r_{ij}^2$ 

where  $r_{ij}^2$  is the square of the distance between the landmarks i and j

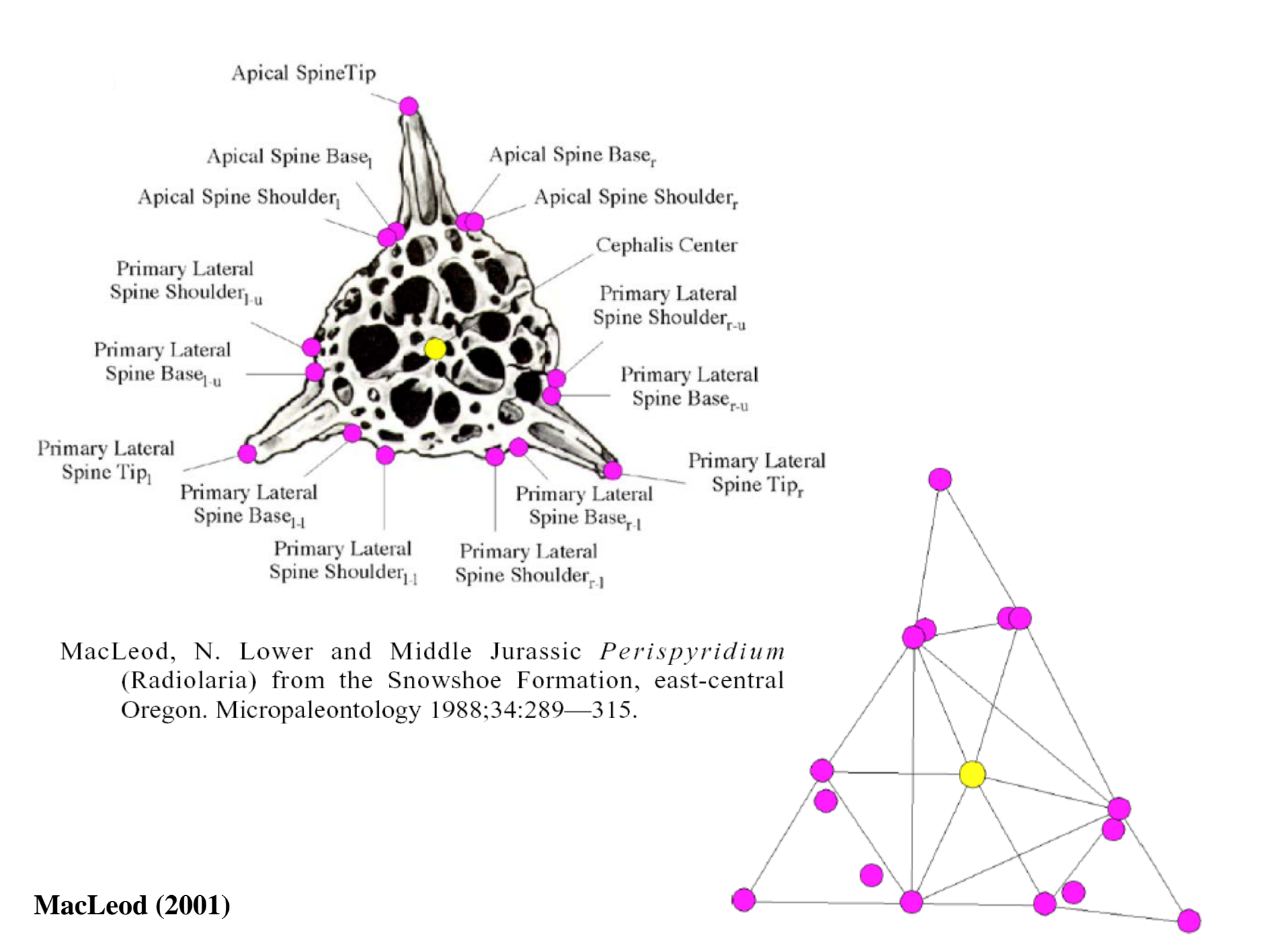
for the matrix 
$$\mathbf{Q}$$
, it holds that  $\mathbf{Q} = \begin{bmatrix} 1 & x_1 & y_1 \\ 1 & x_2 & y_2 \\ \vdots & \vdots & \vdots \\ 1 & x_p & y_p \end{bmatrix}$ 

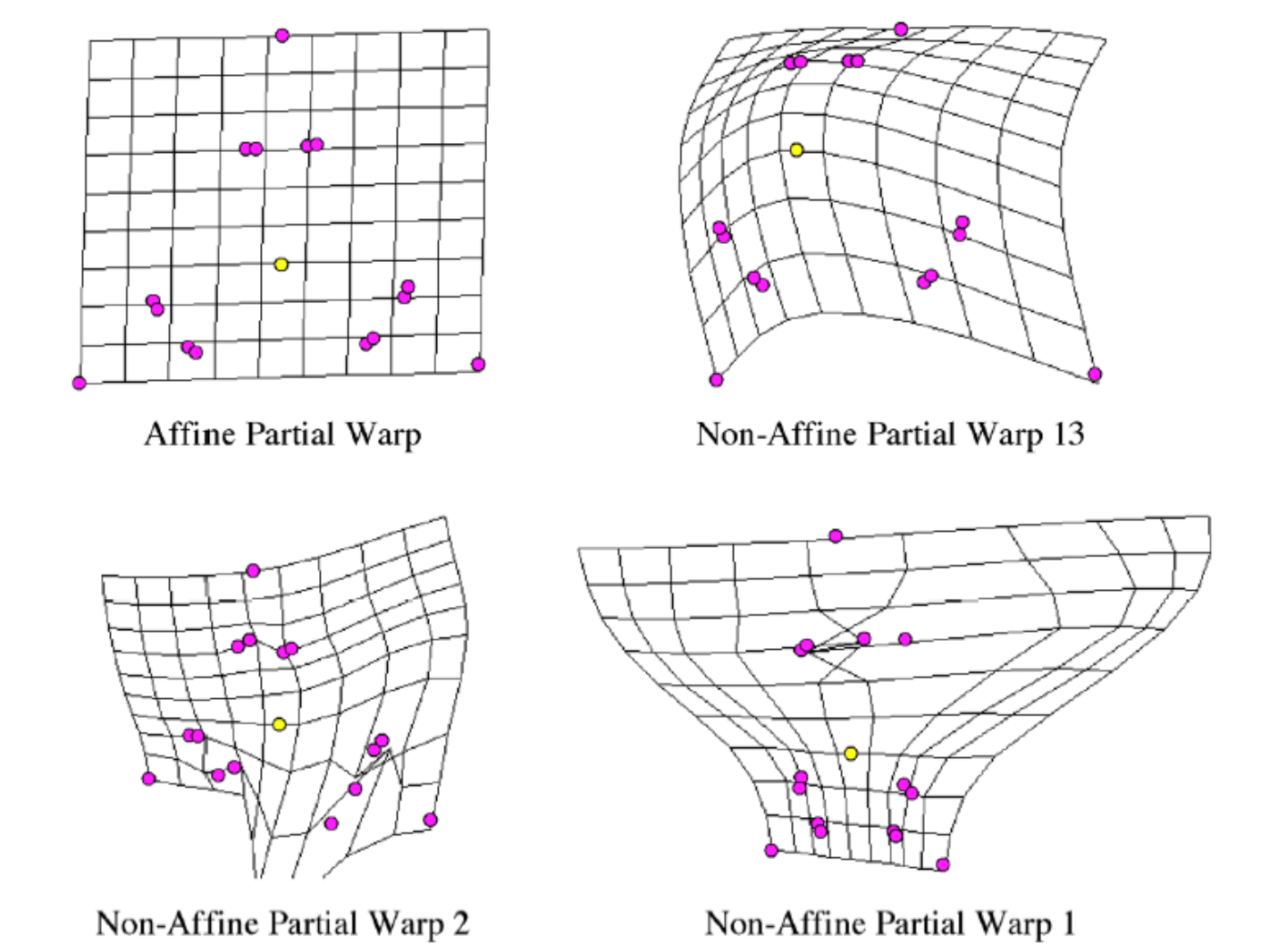
and where x and y are the coordinates of the landmarks of the reference object

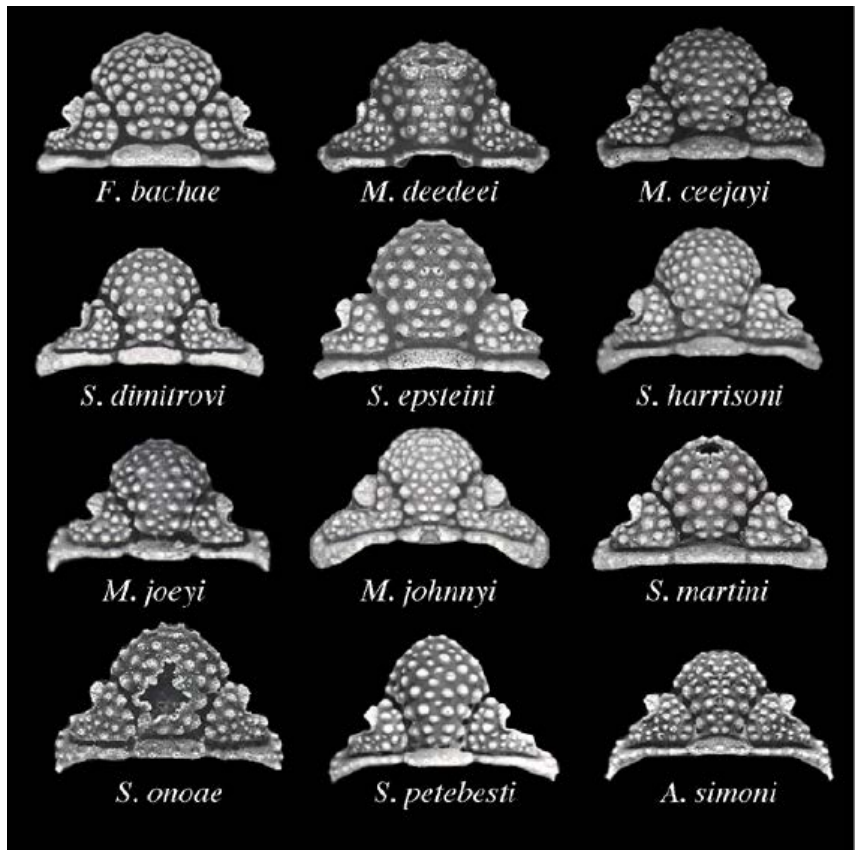
- The decomposition of the deformation energy matrix yields mutually orthogonal eigenvectors called partial warps.
- Partial warps depend on the configuration of the reference object for example, omitting a single landmark will change the "pattern" of all deformations.
- The analogy with PCA (it also involves "eigenanalysis") is not complete because here we work with only one object.
- The values of the corresponding eigenvalues of the deformation energy matrix depend on the degree of localization of the respective transformation. The larger the eigenvalue, the more localized and "energetically demanding" the respective change is. The first three eigenvalues are zero because they correspond to affine shape changes.

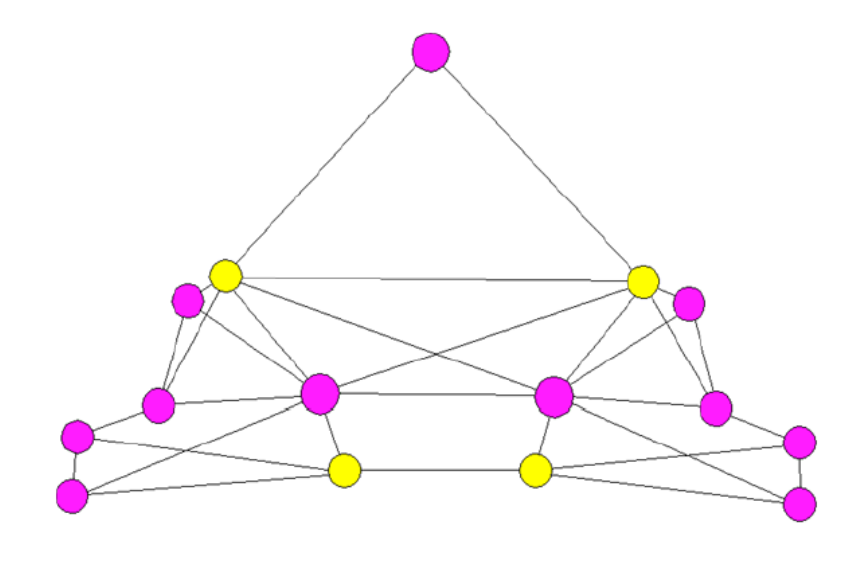
- Partial warps by themselves do not characterize the change; they are merely a system of coordinates (axes) that define the space in which we analyze shape changes.
- The scores of partial warps for a given object indicate the position of that object relative to the reference object along the partial warps.
- For each object, we obtain p-3 values (partial warp scores) for the x and y axes (or for the x, y, z axes in three-dimensional objects). For mm objects, we then obtain either  $m \times 2(p-3)$  or  $m \times 3(p-3)$  values

- Principal warps refer to deformed surfaces (warped surfaces, thin plate splines) and are eigenfunctions of the deformation energy matrix.
- Partial warps are projections of principal warps onto a plane defined by the *x* and *y* coordinates figuratively speaking, they are the "shadow" of the principal warps on the plane defined by *x* and *y* coordinates.
- Principal warps, like partial warps, are derived solely from the reference object.







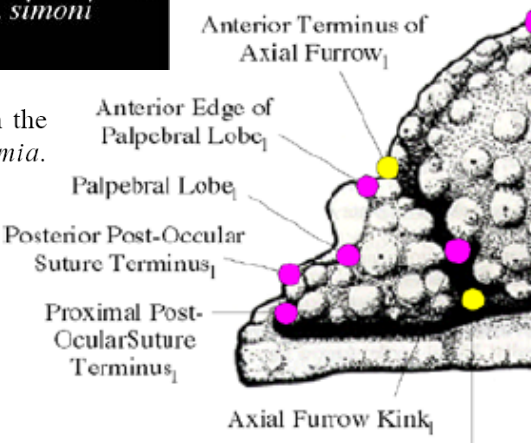


Anterior Terminus of Axial Furrow,

Antro-Median Point

Figure 1. Representative trilobite cranidia from species in the genera *Struszia*, *Mackenziurus*, *Avalanchurus*, and *Fammia*.

Adrain, JM, and Edgecombe, GD. Silurian encrinurine trilobites from the central Canadian Arctic. Palaeontographica Canadiana 1997;14:1—109.



Palpebral Lobe

Anterior Edge of

Palprebral Lobe,

Posterior Post-Ocular Suture Terminus,

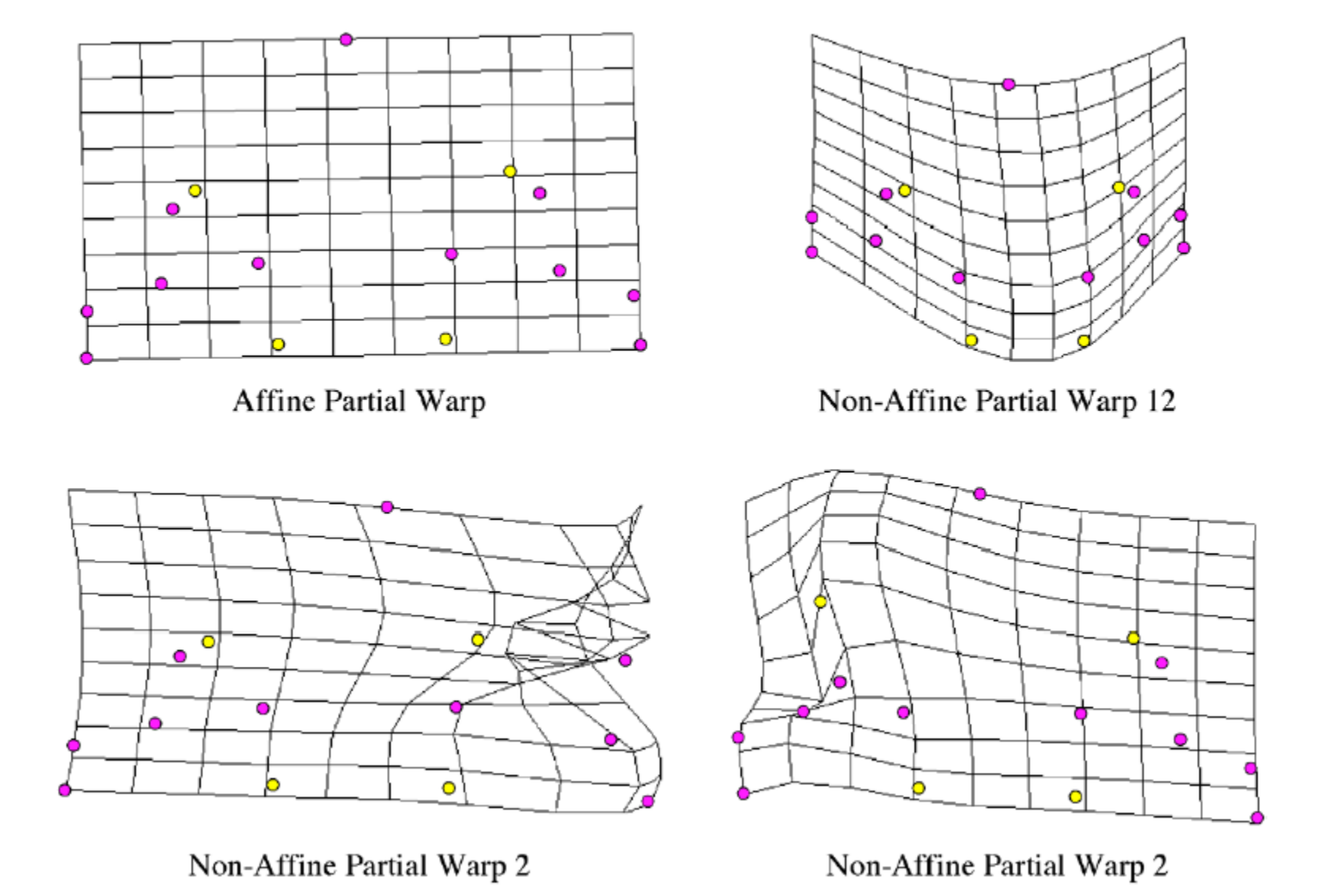
> Proximal Post-Ocular Suture Terminus,

Axial-Occiplital Furrow Junction

Axial-Ociplital Furrow Junction,

Axial Furrow Kink,

MacLeod (2001)



As taxonomic features or values of objects on an ordination diagram that define relationships between objects, relative warps can be used.

These are calculated from the matrix of partial warps of size  $m \times 2(p-3)$  or  $m \times 3(p-3)$  using principal component analysis (here referred to as relative warp analysis) based on the covariance matrix. The values for individual objects on the principal components (relative warps) express the degree of difference in their shapes.

Relative warps can also be interpreted as the principal components of the shape distribution in a space that is tangentially positioned to Kendall's space.

- The values of partial warps can be adjusted before calculating relative warps using the coefficient  $\alpha$ :

-  $\alpha > 0$  – global warps with lower energy levels have greater weight.

-  $\alpha$  < 0 – local warps with higher energy levels have greater weight.

- Values from the interval -1 to +1 are used.

Relative warps can also be calculated directly from Procrustes "residuals" – from vectors connecting the landmarks of the compared object and the consensus configuration after their superposition (the sum of the squared lengths of these vectors is approximately equal to the squared Procrustes distance between the compared object and the consensus configuration in Kendall's space).

It holds that the sum of the squared scores of partial warps is equal to the squared Procrustes distance from the reference object.

# Use of Geometric Morphometrics to Differentiate *Gila* (Cyprinidae) within the Upper Colorado River Basin<sup>1</sup>

Michael E. Douglas, Marlis R. Douglas, John M. Lynch, and Douglas M. McElroy

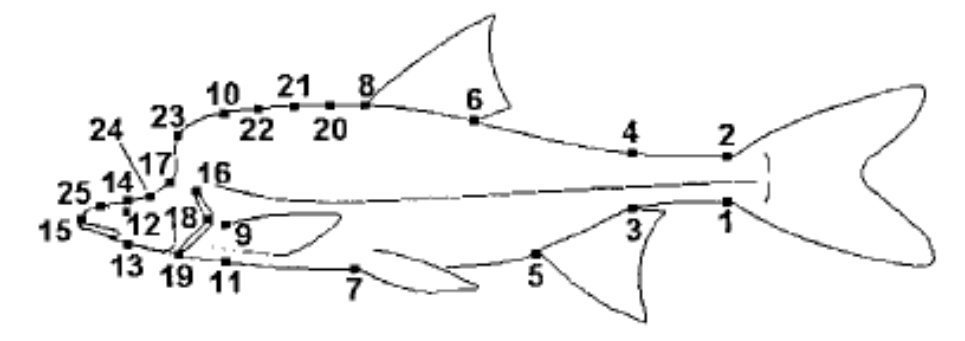


Fig. 1. Landmarks used in the current study. Definitions are given in text or in McElroy and Douglas (1995).

TABLE 1. MATERIAL EXAMINED.

Codes	Gila cypha	Gila robusta
BR	25	19
CC	11	6
DC	22	24
LC	28	_
ww	57	56
YR	5	65
DB	_	20
RI	_	25
	BR CC DC LC WW YR DB	BR 25 CC 11 DC 22 LC 28 WW 57 YR 5 DB —

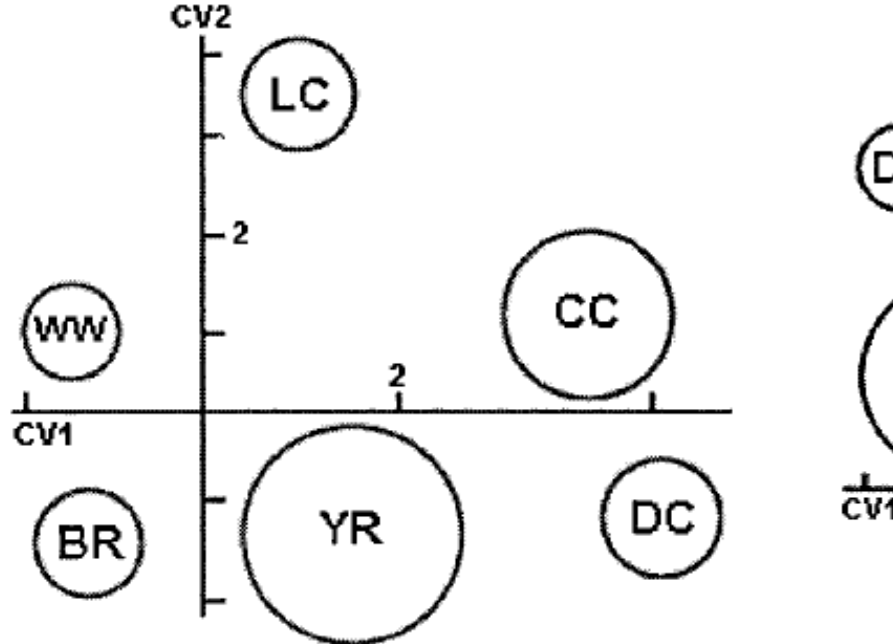


Fig. 2. Shape variation among six *Gila cypha* populations based on the first two variates derived from a canonical analysis of shape coordinates. Population abbreviations follow Table 1. Circles represent 95% confidence intervals for the group mean.

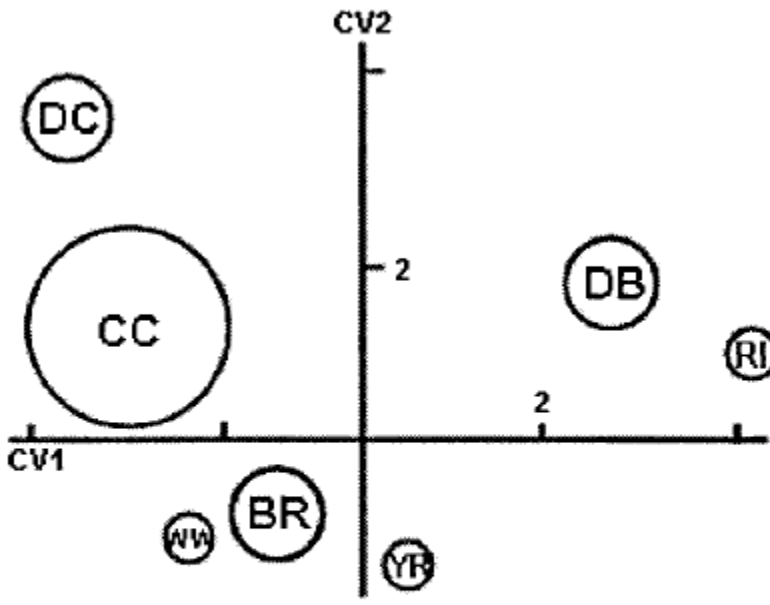


Fig. 3. Shape variation among seven *Gila robusta* populations based on the first two variates derived from a canonical analysis of shape coordinates. Population abbreviations follow Table 1. Circles represent 95% confidence intervals for the group mean.

Table 2. Classification Results for Gila cypha from a Canonical Analysis of Shape Coordinates. Numbers in parentheses are classification results from truss analysis of McElroy and Douglas (1995). Key to sample codes is given in Table 1.

	BR	CC	DC	LC	ww	YR
BR	24 (24)	0 (0)	0 (0)	0 (0)	1 (1)	0 (0)
CC	0 (0)	11 (11)	0 (0)	0 (0)	0 (0)	0 (0)
DC	0(0)	0(0)	22 (22)	0(0)	0(0)	0(0)
LC	0(0)	0(0)	0(0)	28 (28)	0 (0)	0(0)
WW	3(1)	0(0)	0(0)	0(1)	54 (55)	0(0)
YR	0 (0)	0 (0)	0 (0)	0 (0)	0 (0)	5 (5)

Table 3. Classification Results for *Gila robusta* from a Canonical Analysis of Shape Coordinates. Numbers in parentheses are classification results from truss analysis of McElroy and Douglas (1995). Key to sample codes is given in Table 1.

	BR	CC	DC	ww	YR	DB	RI
BR	19 (18)	0 (0)	0 (0)	0 (0)	0 (1)	0 (0)	0 (0)
CC	0 (0)	6 (6)	0 (0)	0 (0)	0 (0)	0 (0)	0 (0)
DC	0 (0)	0 (0)	24 (24)	0 (0)	0 (0)	0 (0)	0 (0)
WW	2 (0)	0 (0)	0 (0)	52 (52)	2(1)	0(2)	0 (0)
YR	3 (1)	0 (0)	0 (0)	0 (0)	62 (63)	0 (1)	0 (0)
DB	0 (0)	0 (0)	0 (0)	0 (0)	0 (1)	20 (19)	0 (0)
RI	0 (0)	0 (0)	0 (0)	0 (0)	1 (1)	0 (0)	24 (24)

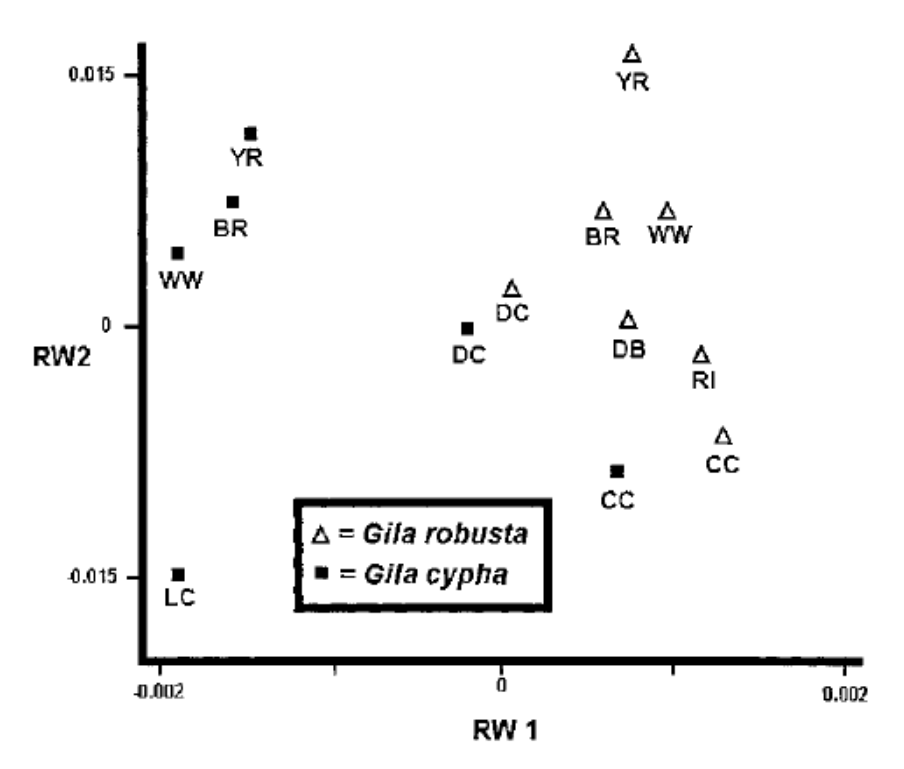


Fig. 4. Shape variation among 13 populations of *Gila cypha* and *Gila robusta* based upon the first two relative warps (RWs) of a relative warp analysis of shape coordinates using the grand mean as the tangent configuration. Population abbreviations follow Table 1.

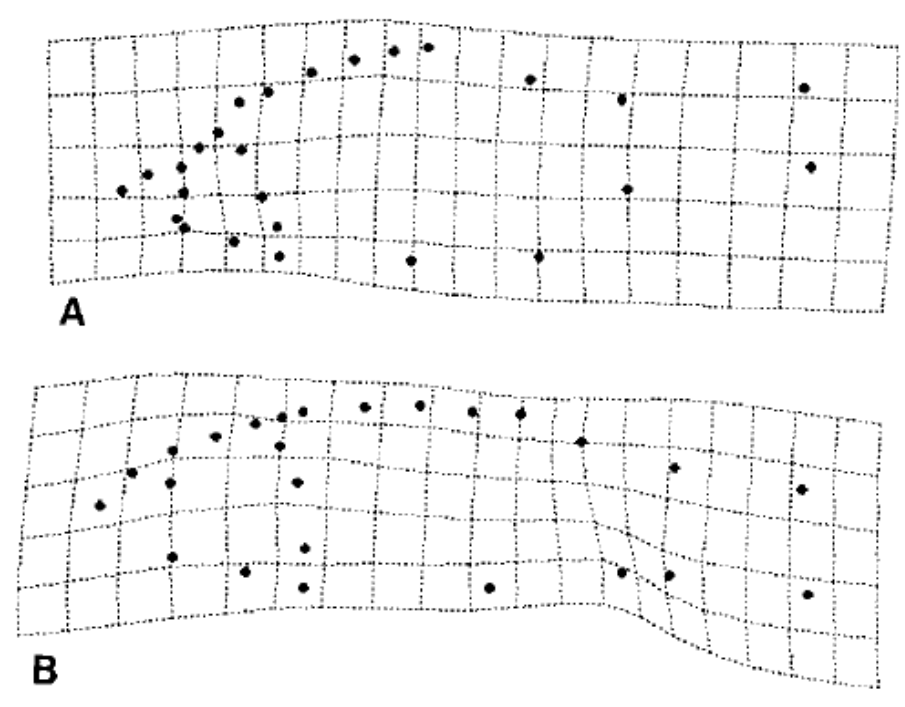


Fig. 5. Splines illustrating shape variation among the first relative warp axis of Figure 4. (A) corresponds to negative values of the warp and depicts a phenotype indicative of *Gila cypha*; (B) corresponds to positive values of the warp and demonstrates a *Gila robusta* phenotype.

## INTEGRATING DEVELOPMENTAL EVOLUTIONARY PATTERNS AND MECHANISMS: A CASE STUDY USING THE GASTROPOD RADULA

#### R. P. GURALNICK<sup>1,2</sup> AND D. R. LINDBERG<sup>1</sup>

<sup>1</sup>Department of Integrative Biology and Museum of Paleontology, University of California, Berkeley, California 94720-4780 <sup>2</sup>E-mail: robg@ucmp1.berkeley.edu

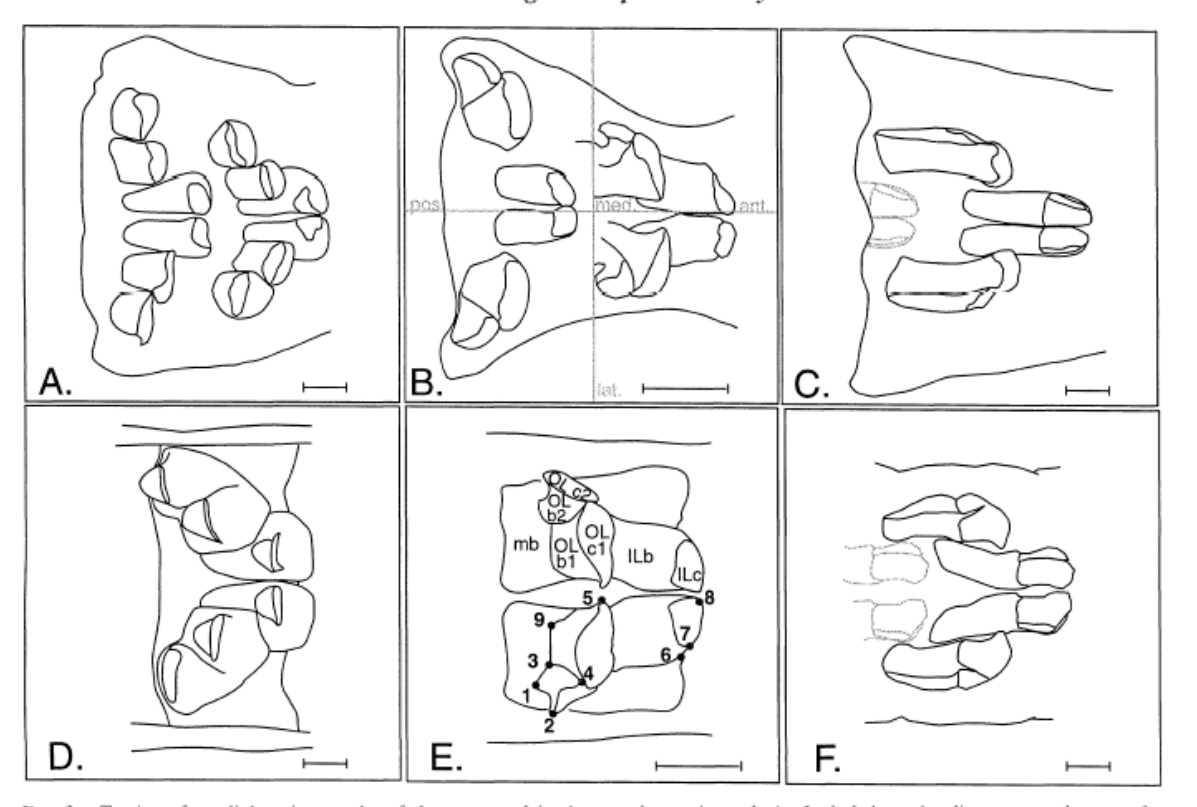
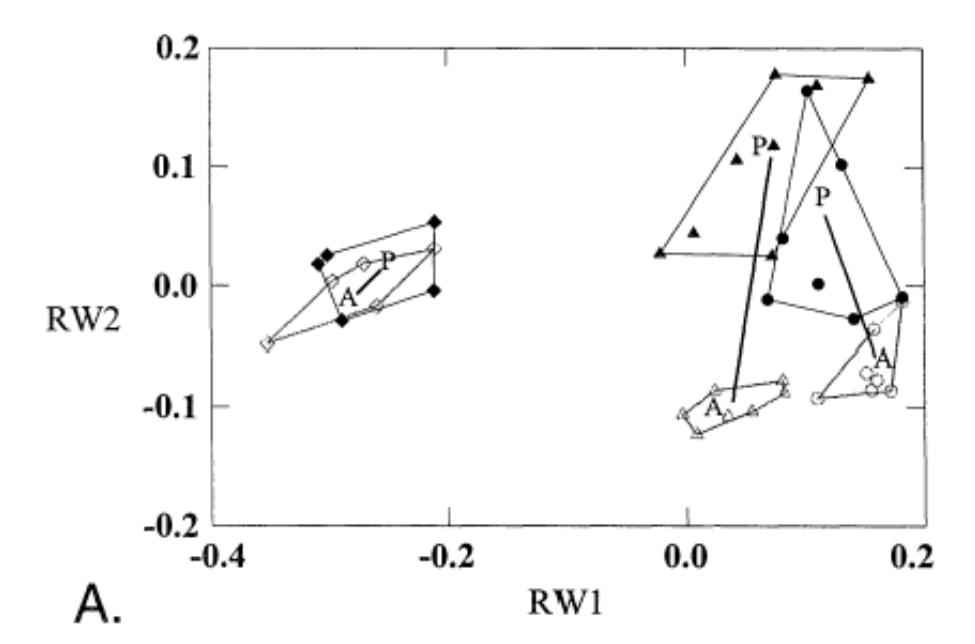


Fig. 3. Tracings from light micrographs of the taxa used in the morphometric analysis. Included on the diagram are the axes for orientation (anteroposterior and mediolateral), landmarks used in the study and labels showing the names of different elements. (A) Posterior two radular rows of Acmaea mirra. (B) Posterior two rows of Lottia ceciliana as well as axes. (C) Second-most posterior row of Nacella concimaa. Teeth in gray are the ILs of the next most posterior row. (D) Anterior row of A. mitra. (E) Anterior row of L. ceciliana showing the nine landmarks used in the analysis on one side and labels of the subparts of the radula on the other. (F) Anterior row of N. concimaa. ILc, IL cusp; ILb, IL base; mb, membrane plate; OLb1, the medial outer lateral base; OLb2, the lateral outer lateral base; OLc1, the medial cusp of the outer lateral; OLc2, the lateral cusp of the outer lateral. Scale bar = 100 µm.



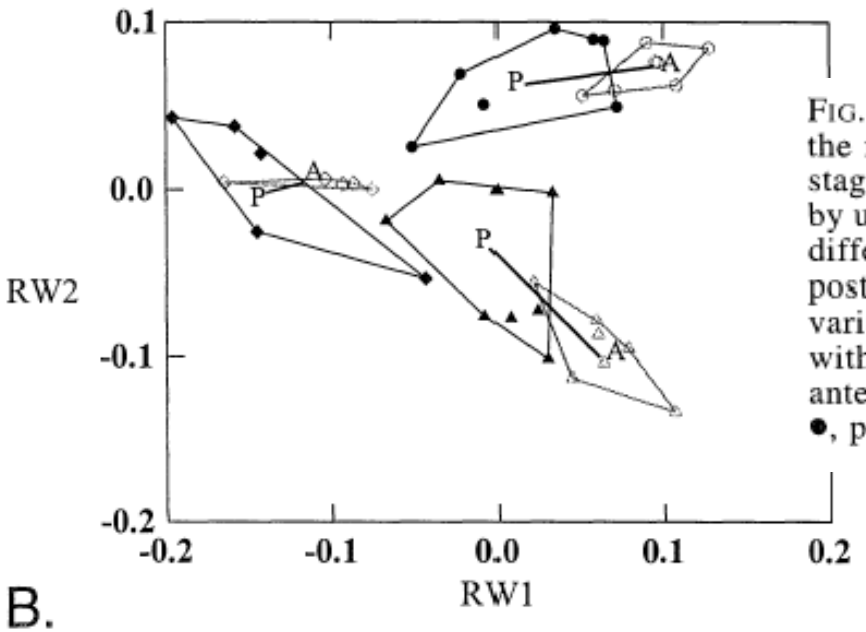


Fig. 4. Bivariate scatterplot for the relative warps axes that explain the most variation in the sample. We have grouped by ontogenetic stage and by taxon. Anterior rows and posterior rows are represented by unfilled and filled symbols respectively. Taxa are represented by different symbols. We draw trajectories between the anterior and posterior clusters for each taxon to show general patterns. (A) Bivariate plot with uniform component included. (B) Bivariate plot with uniform component excluded. ♠, posterior row Nacella; ♦, anterior row Nacella, ♠, posterior row Lottia; ♠, anterior row Lottia; ♠, posterior row Acmaea; ○ anterior row Acmaea.

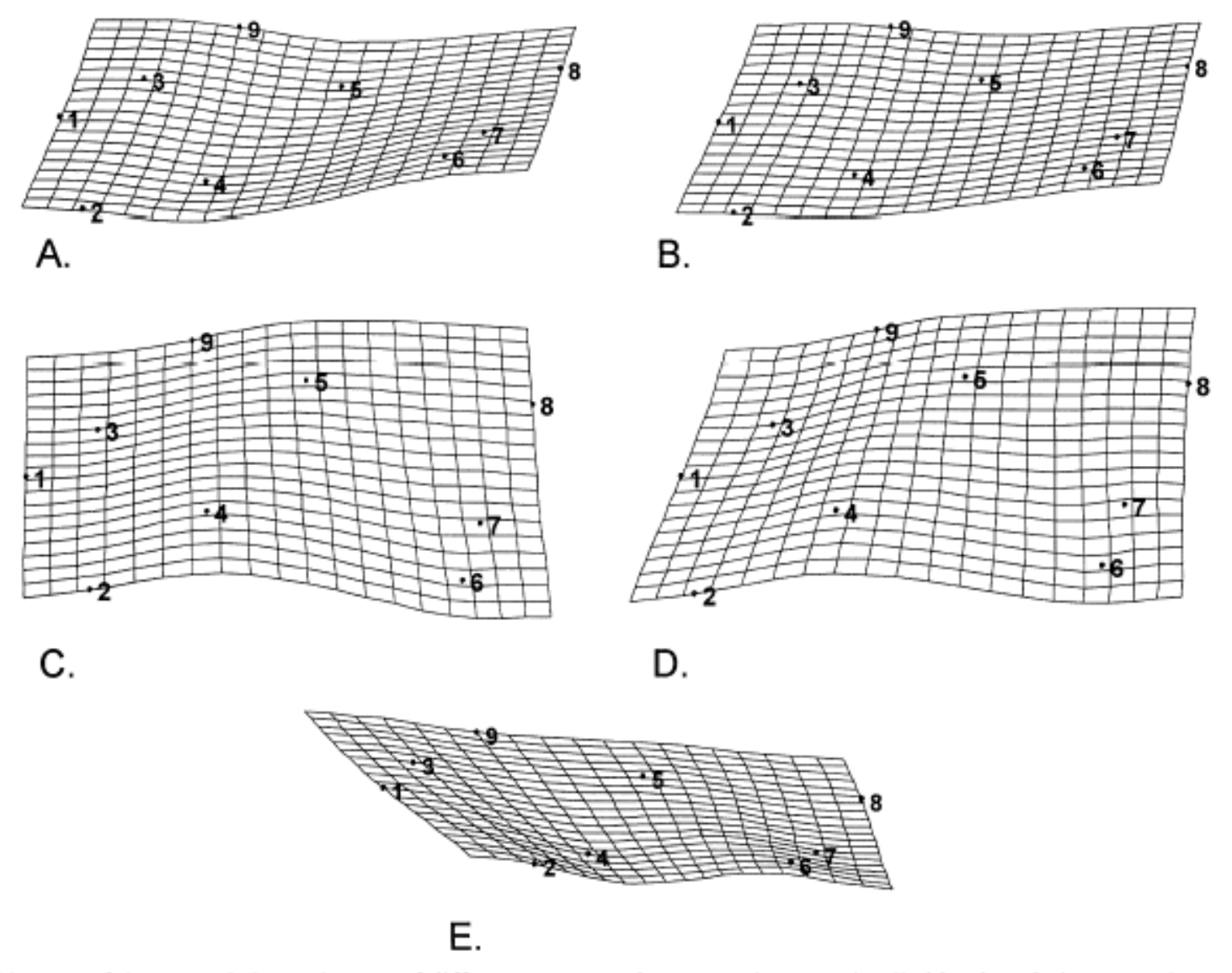
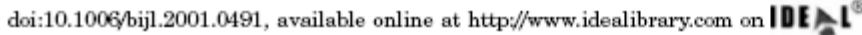


Fig. 5. Diagram of the general shape changes of different groups and ontogenetic stages implied by the relative warp shape space with the uniform component included (Fig. 4A). Shape change for (A) Lottia posterior rows; (B) Acmaea posterior rows (C) Lottia anterior rows; (D) Acmaea anterior rows; (E) Nacella posterior and anterior rows.





#### The species delimitation problem applied to the Agabus bipustulatus complex (Coleoptera, Dytiscidae) in north Scandinavia

MARCUS K. DROTZ\* and ANSSI SAURA

Department of Molecular Biology/Genetics, Umeå University, SE-901 87 Umeå, Sweden

#### ANDERS N. NILSSON

Department of Ecology and Environmental Science, Umeå University, SE-901 87 Umeå, Sweden

#### MORPHOLOGICAL CHARACTERS

Twelve adult morphological characters were analysed with a Wild M3C dissecting microscope (Heerbrugg 310345) and a Wild  $10\times21B$  eyepiece graticule (Heerbrugg 445111). The specimens were killed in 70% ethanol and pinned prior to analysis. The following characters were studied at  $40\times$  magnification; HSW, PSW, ESW and PS, and at  $25\times$  magnification; PL, WS, FL and FW (for explanation, see Table 2). The primary reticulation of the beetle consists of small uniform hexagonal meshes, and the secondary reticulation consists of oblong meshes delimited by coarse impressed lines.

Thirteen landmarks were chosen for the TSRWA:

- Pronotum, left anteriolateral angle.
- (2) Pronotum, mid point between landmarks 1 and 3.
- (3) Pronotum, left posteriolateral angle.
- (4) Left elytron, posterior apex.
- (5) Right elytron, posterior apex.
- (6) Pronotum, right posteriolateral angle.

- (7) Pronotum, mid point between landmarks 6 and 8.
- (8) Pronotum, right anteriolateral angle.
- (9) Pronotum, central anterior margin.
- (10) Pronotum, central posterior margin.
- (11) Scutellum, posterior apex.
- (12) Right elytron, lateral point at widest portion.
- (13) Left elytron, lateral point at widest portion.

The head was not included because its flexibility could affect the outcome of the analysis (Nilsson, 1985; Ribera & Nilsson, 1995). The landmarks were digitized on to a Summa Sketch III (Summagraphics) graphics tablet.

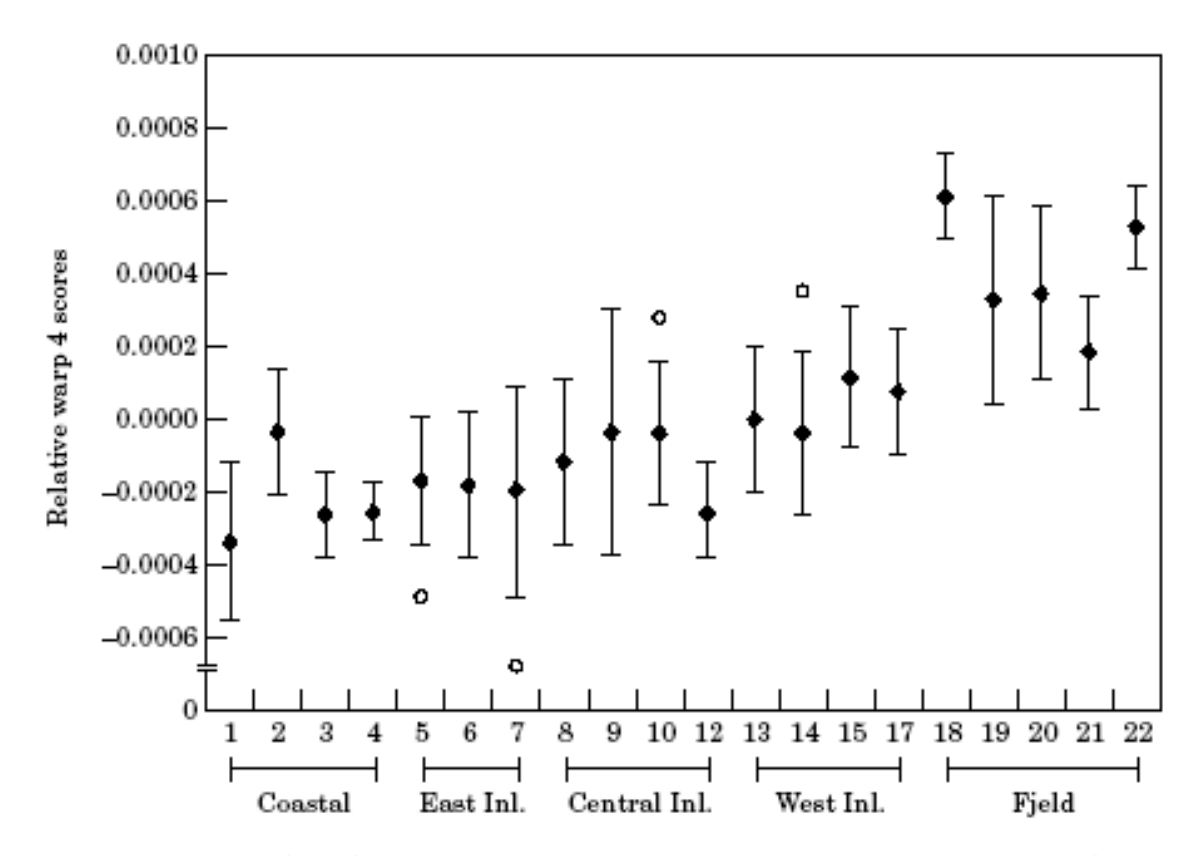


Figure 2. Female relative warp 4 (RW4) scores for each locality in the transect, except 11 and 16 because of too few females. The outlier  $(\bigcirc)$  is defined with an outlier coefficient of  $1.5 \times$  the difference of the upper and lower levels of the mean  $(\spadesuit)$  and standard error.

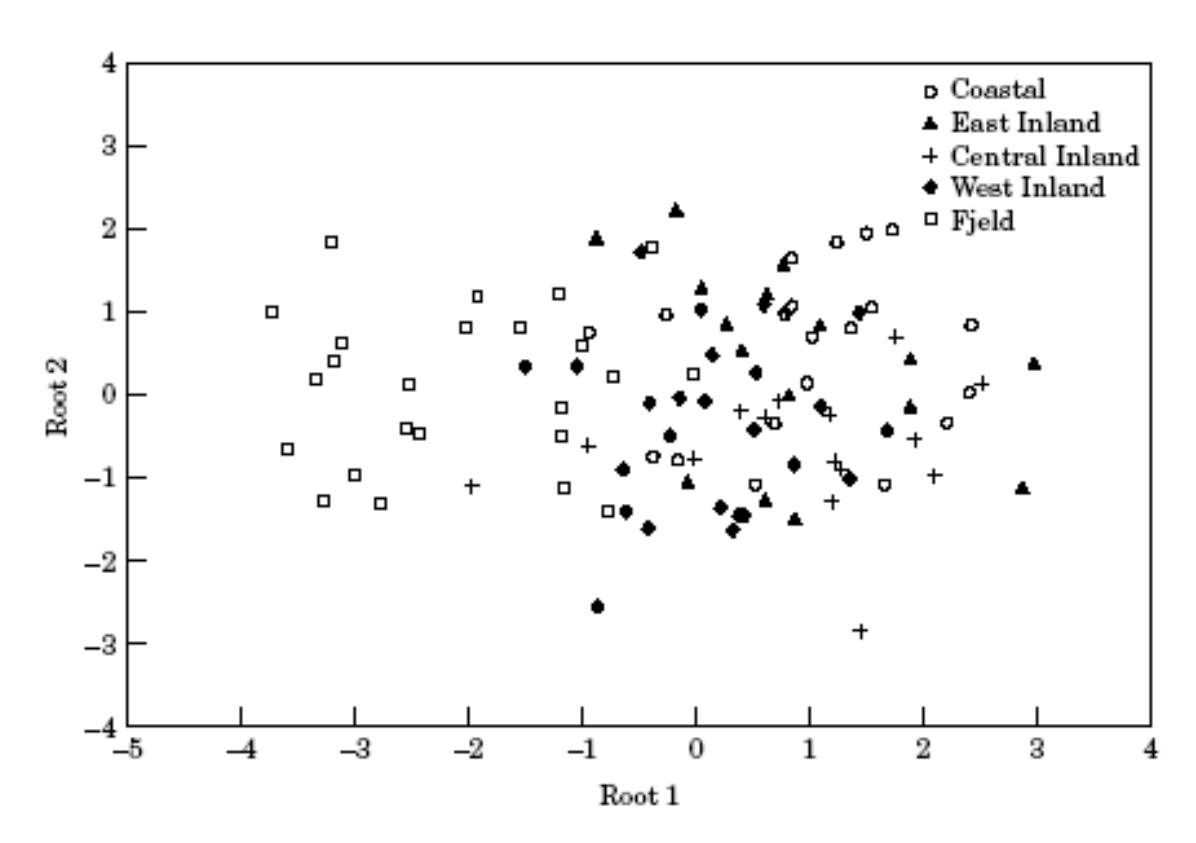


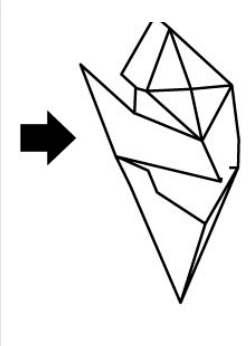
Figure 1. Scores plot from the females' Canonical Variates Analysis (CVA) landmark analysis, showing the large overlaps between the different regions.

# 10 8 0 6 10 80 12 15 16°

#### Quantifying temporal bone morphology of great apes and humans: an approach using geometric morphometrics

Charles A. Lockwood, 1 John M. Lynch2 and William H. Kimbel1

<sup>1</sup>Department of Anthropology & Institute of Human Origins, and <sup>2</sup>Barrett Honors College & Institute of Human Origins, Arizona State University, Tempe, AZ 85287, USA



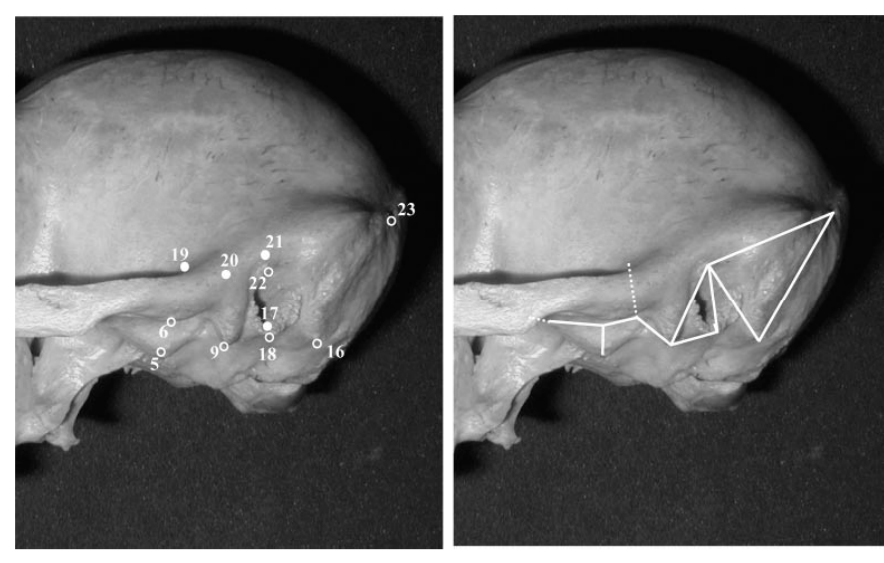
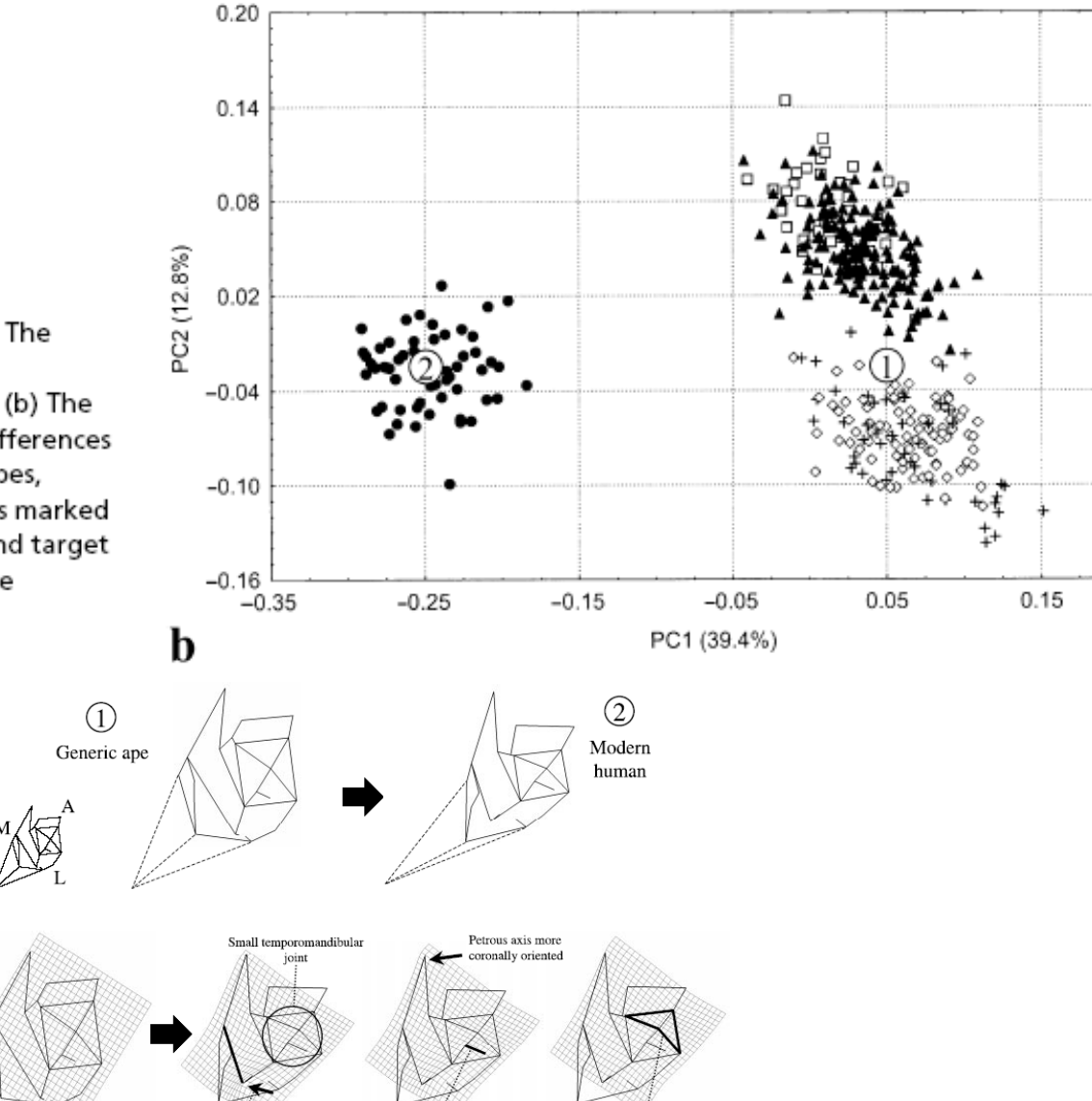


Fig. 1 Landmarks used in this study, labelled on a chimpanzee cranium in inferior view (above) and lateral view (below). Numbers correspond to those given in Table 2. Some landmarks (open circles) are labelled in both views. Temporal bone form is illustrated by use of wireframe diagrams linking landmarks, as shown in the panels on the right.

Fig. 3 PCA of all hominids. (a) The first three PCs summarize the differences among all species. (b) The analysis is dominated by the differences between humans and great apes, as described by PC1. The points marked '1' and '2' are the reference and target shapes for the thin-plate spline transformation illustrated in Figs 5 and 6.



Preglenoid surface

strongly compressed

0.25

Fig. 5 Thin-plate spline transformation between apes and modern humans. Inferior view. Numbers correspond to those given in Fig. 3 and indicate the position of the reference and target shapes in the PCA. Dashed lines indicate the position of asterion, for display purposes. That landmark is not incorporated into the analysis. In this and all spline figures, different positions of the spline are shown, highlighting different aspects of the transformation. The labelled features are human traits.

Tympanic element less laterally extended

(more sagittally oriented)

Mandibular fossa medially positioned

relative to braincase

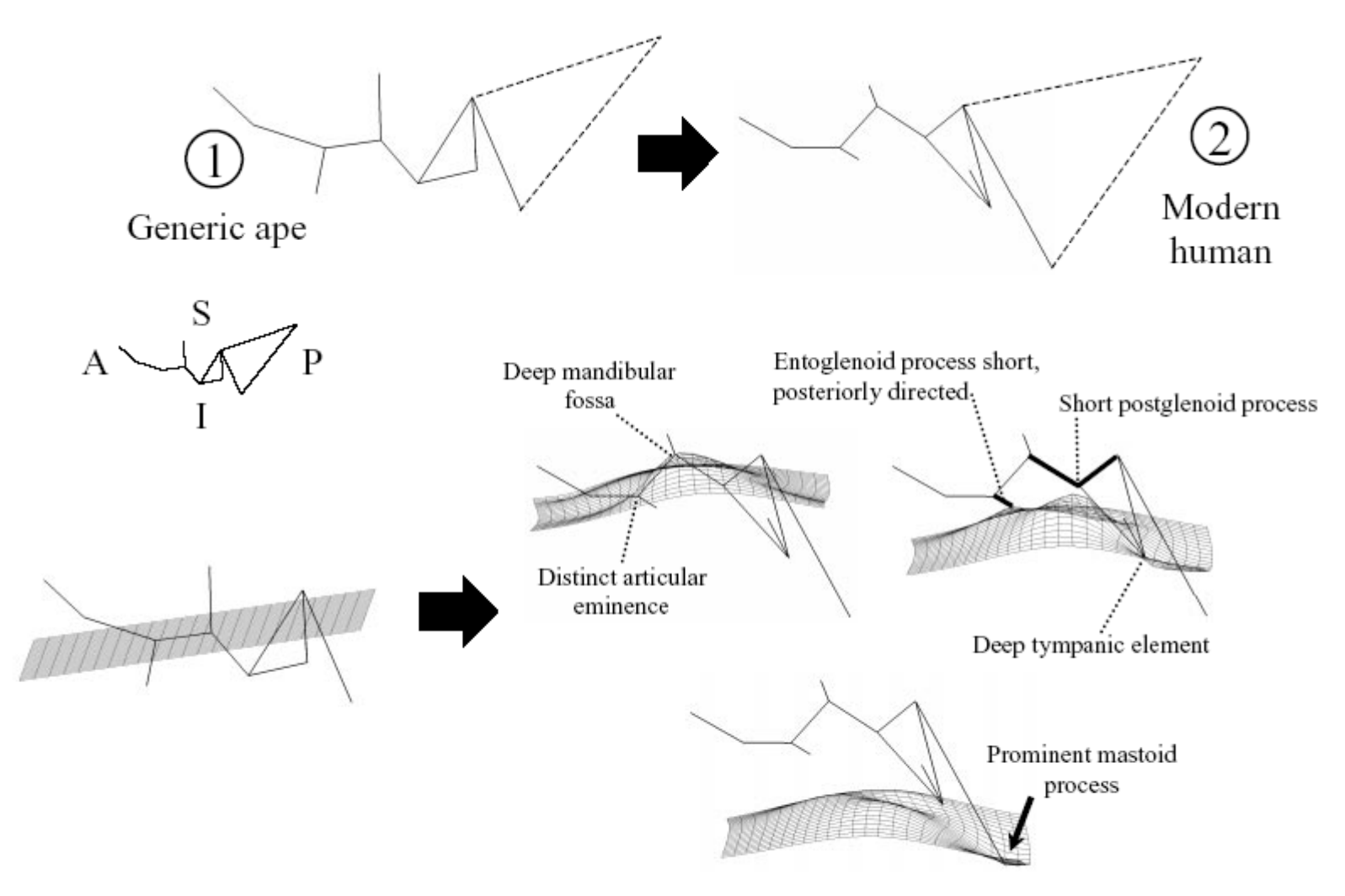


Fig. 6 Thin-plate spline transformation between apes and modern humans. Lateral view. Numbers correspond to those in Fig. 3 and indicate the position of the reference and target shapes in the principal component analysis. Dashed lines indicate the position of asterion, for display purposes. That landmark is not incorporated into the analysis. Some human characteristics are indicated.

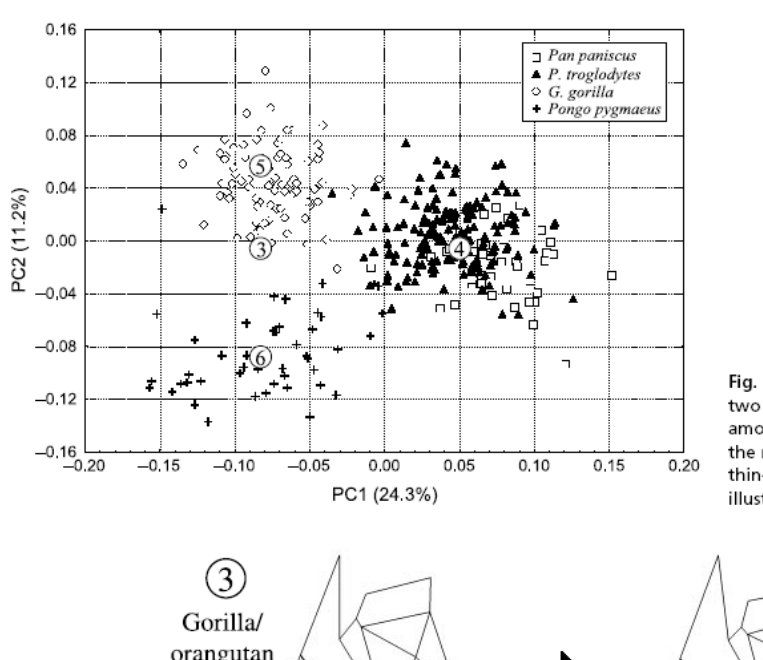


Fig. 7 PCA of the great apes. The first two PCs summarize the differences among species. The numbered points are the reference and target shapes for the thin-plate spline transformations illustrated in Figs 9 and 10.

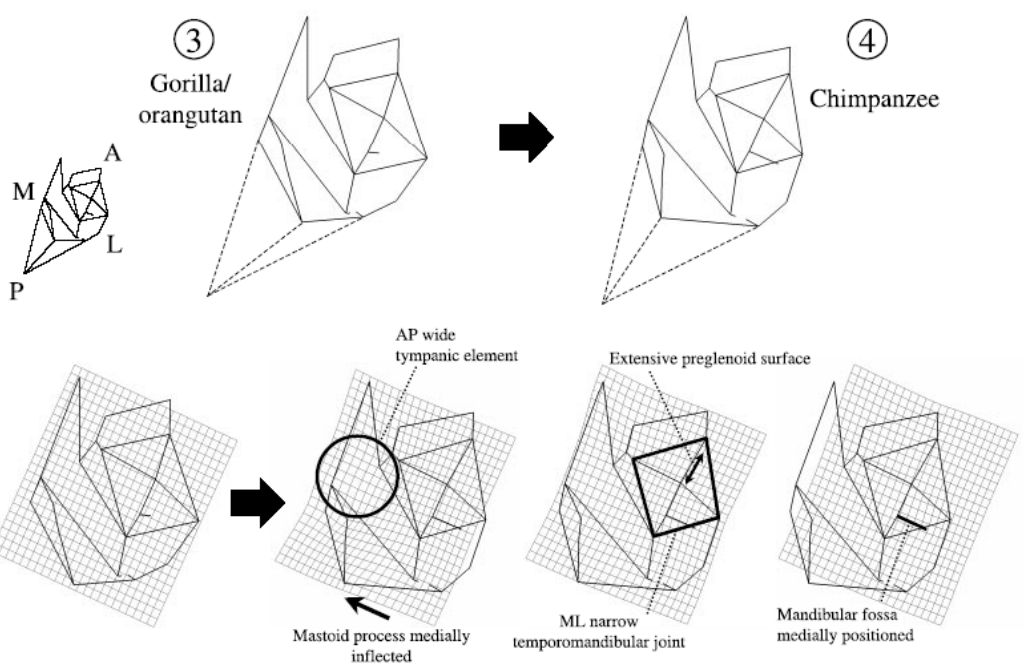


Fig. 8 Thin-plate spline transformation between a reference shape phenetically intermediate between *Gorilla* and *Pongo*, and a target shape at the *Pan troglodytes* centroid. Inferior view. Numbers correspond to those in Fig. 7 and indicate the position of the reference and target shapes in the PCA. Dashed lines indicate the position of asterion, for display purposes. That landmark is not incorporated into the analysis.

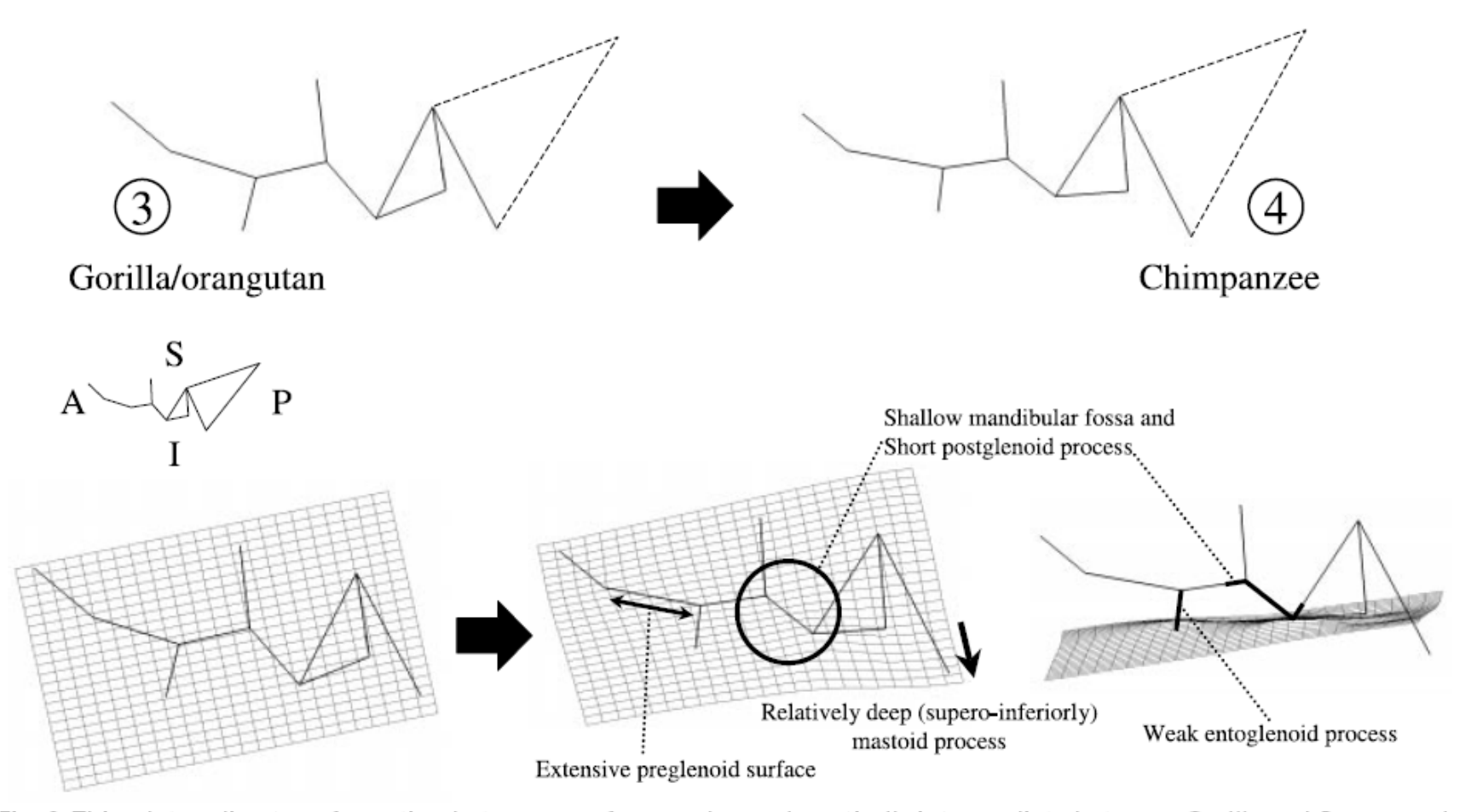


Fig. 9 Thin-plate spline transformation between a reference shape phenetically intermediate between *Gorilla* and *Pongo*, and a target shape at the *Pan* centroid. Lateral view. Numbers correspond to those in Fig. 7 and indicate the position of the reference and target shapes in the principal component analysis. Dashed lines indicate the position of asterion, for display purposes. That landmark is not incorporated into the analysis.